Aerospace Science and Technology 148 (2024) 109080

Contents lists available at ScienceDirect

Aerospace Science and Technology

journal homepage: www.elsevier.com/locate/aescte

Multiobjective aerostructural optimization for efficient transport wing conceptual design

Spyridon G. Kontogiannis [a,*,1], A. Mark Savill [a,1], Vasileios Mazis [b], Vangelis Skaperdas [b]

[a] Cranfield University, Bedfordshire, MK430AL, United Kingdom
[b] BETA CAE Systems, Thessaloniki, Greece

ARTICLE INFO

Communicated by Yongle Du

ABSTRACT

The advantages of Multidisciplinary wing development are only gradually being exploited in an industrial level, largely halted by the inevitable design space complexity arising from the interacting disciplines and objective constraints. An industrial tool has to provide design space exploration early in the design process and be reliable enough to guide subsequent fine-tuning optimization studies. In this paper, we display how our methodology can be used in an industrially relevant constrained aerostructural problem described by the common research model and formulated by the asymmetric subspace optimization architecture. It uses multi fidelity analyses in a surrogate based optimization framework, offering more detailed information earlier in the design cycle. The results indicate efficient space exploration, particularly due to the system level dimensionality reduction associated with such a load balancing architecture.

1. Introduction

Over the past decades, the aerodynamic design of conventional configurations has matured to a point where performance is currently reaching a plateau. With limited room for ground-breaking leaps, industrial steps forward are the accumulative result of successive disciplinary improvements, typically involving a leading discipline dictating the rest of the design decisions and disciplines. However, under this approach the sub-systems' and overall system's performance is reduced. Improving interdisciplinary synergy is essential to break through this development plateau and configurations driven by global merit through parallel subsystems development prove superior. There is an abundance of Multidisciplinary Design Optimization (MDO) applications on wing design [1–7] showing how MDO is more efficient than aerodynamic based design due to inward loads shifting allowing for a lighter structure.

However, the development of multidisciplinary studies [8,9] raises further complexities in the optimization process, inherent to the disciplines and interdisciplinary communication. These can be split in two categories; introduced by the multidisciplinary analysis (MDA) or by the optimisation of the multidisciplinary (MD) systems. An example of interdisciplinary communication complication is found in an aerostructural analysis which is a specific case of a fluid-structure interaction (FSI) problem. Typically, aerostructural optimization requires a form of MDA. During the analysis, direct exchange of information is demanded, namely pressure loads and structural displacements. Unless a single analysis code is used for both disciplines (fully coupled approach) the multidisciplinary analysis is split in two distinctive analysis codes (loosely coupled approach). Each one involves its own computational domain, resulting to a non-matching disciplinary interface that demands the use of an additional algorithm to properly distribute the quantities of interest between the grids. Typical examples of such algorithms include the method of Brown [10] based on rigid links, the nearest neighbour interpolation (NNI) [11], Galerkin [12–14] and Radial Basis Function (RBF) functions for generating the interpolation models [15–17]. The grid nodes are essentially considered as "sets of point clouds", no grid connectivity information is necessary and as such, the method can be used within any type of grids. The various methods available to tackle the mapping problem are briefly reviewed by Rendall [18]. An extensive review is provided by Guruswamy [19] and de Boer et al. [20].

Another significant requirement arising by the MDA, is robust grid deformation. Relevant methods are categorized into structured and unstructured depending on their target topology. Structured grids, typ-

* Corresponding author.
E-mail address: spkontogiannis@gmail.com (S.G. Kontogiannis).
[1] School of Aerospace, Transport and Manufacturing, Propulsion Engineering Centre.

https://doi.org/10.1016/j.ast.2024.109080
Received 3 December 2023; Received in revised form 3 March 2024; Accepted 14 March 2024
Available online 21 March 2024
1270-9638/© 2024 The Authors. Published by Elsevier Masson SAS. This is an open access article under the CC BY license (http://creativecommons.org/licenses/by/4.0/).

ically use the transfinite interpolation (TFI) [21] or any variation of the linear elasticity or algebraic family of methods [22], whereas concepts — for multiblock grids — are provided by Soni [23] and extended by Jones and Samareh [24]. Unstructured grids methods might employ a physical concept analogy like linear [25] and torsional springs [26,27], or the heat conduction equation [28] to model the nodes' movement [29]. Beckert and Wendland [17], De Boer et al. [30] and recently Abergo et al. [31], used an RBF based approach that does not require grid connectivity information and can be unified with the RBF based mapping technique to create a unified methodology for aeroelastic [18] simulations. Mi et al. [32] used a variation of Free Form Deformation (FFD) for geometry and mesh deformation. An overview of grid deformation methods is provided by Samareh [33].

Increasing the number of disciplines increases the complexity and the cost of the optimization process as more variables are required to describe the problem. Furthermore, it introduces a more multimodal design space because of interdisciplinary interactions [34]. In popular approaches like the surrogate model optimization (SBO) which are used in a variety of applications [35–38], this cost increase is known as the 'curse of dimensionality'. Alternatively, adjoint formulations do not suffer from this scalability problem as their computational cost is analogous to the number of objective functions instead. When used in MDO, typical practice involves a single objective (SO) incorporating multidisciplinary information — such as the Breguet equation [39] or a weighted function [40] — and structural considerations [41,42]. However, their local search character limits the multidisciplinary synergy benefits. To get the maximum from an MDO study, early stage exploration is preferable to identify sets of promising and diverse trends. In such a stage there is scope for data driven models [43,44] to provide valuable information to guide optimization studies with reduced cost.

Clearly, there is a need for an MDO scheme to efficiently perform conceptual stage exploration, while offering reliable and mature design information feedback to the engineer. Multifidelity (MF) methods offer such traits and have been applied in a variety of design challenges [45], applications [46–50], on robustness [51] and stability [52]. However, there has not been extensive applications of MF and SBO methodologies on complicated Multiobjective (MO) multidisciplinary problems. The same can be said for the Asymmetric Subspace Optimization architecture [7] (ASO), which despite its benefits in aerostructural problems, has been mostly used in conjunction with low fidelity structural models.

To attack this gap, this work provides an industrially relevant MO application of the ASO architecture with higher fidelity of aerostructural analysis than most implementations. What makes this efficient in a conceptual context, is our novel MF methodology which is based on our modified Kriging and the Expected Improvement (EI) criterion. High fidelity (HF) information is brought earlier in the design stage without penalising the cost. Hence, this paper focuses on illustrating how we can tackle a complex design problem within ASO. For the Multidisciplinary Feasible (MDF) implementation see [53] and for details in our novel MO MF global optimization method see [54].

The wing used is the Common Research Model (CRM) [55], a model specifically developed to approximate the design and physical features of a typical conventional configuration transport wing. Before presenting the optimization problem formulation and the numerical setup of the aerodynamic and structural models, some fundamental considerations on the wingbox structure elements are discussed. Section 2 overviews the optimization methodology and in section 3 the CRM model is described. The optimization problem formulation is presented in Section 4. The results are provided in Section 5 followed by the conclusions in Section 6.

2. Optimization methodology

The methodology employed consists of a multifidelity infill analysis strategy, a modified metamodel so that multifidelity data can be used into a surrogate based optimization plan and an efficient multiobjective optimizer. It acts as a blackbox optimization framework which can subsequently be introduced to any MDO architecture selected for a particular MDO problem. The following sections provide only a brief overview of the method, for more details see [54].

2.1. Multifidelity analyses

To keep computational cost to a minimum while providing reliable design information, we use our MF strategy [54]. An error surrogate $e(\mathbf{x})$ is introduced, trained in design points where both HF and Low Fidelity (LF) results are available. Hence, any subsequent LF prediction y_{LF} can be corrected using this simple superposition [56] scheme to approximate an HF result y_{HF},

$$y_{HF}(\mathbf{x}) = y_{LF}(\mathbf{x}) + e(\mathbf{x}) \tag{1}$$

2.2. Surrogate model

The unavailability of a both accurate and cheap multidisciplinary analysis forbids direct LF calls by a gradient free optimizer. Cost reduction demands SBO, with the optimizer actsing directly on a Kriging model built on a superposition of the LF/HF results - effectively a simple algebraic formulation. This HF objective function prediction mirrors eq. (1) and is defined by,

$$\hat{y}(\mathbf{x}) = \hat{\mu} + \boldsymbol{\psi}^T \boldsymbol{\Psi}^{-1}(\mathbf{y} - \mathbf{1}) + e(\mathbf{x}) \tag{2}$$

In the above, $\hat{\mu}$ is an estimated mean value, $\boldsymbol{\psi}$ and $\boldsymbol{\Psi}$ are the correlation vector and matrix respectively [56]. This simple superposition acts as a mapping of the Kriging predictor, from an approximation of the LF space to that of the HF design space [57]. Therefore, in our novel Kriging implementation, HF points are interpolated whereas the model performs an 'educated' regression near the LF ones. To ensure space filling characteristics, the initial training data (TD) are generated through Latin Hypercub Sampling (LHS) and the Kriging hyperparameters are tuned using a ALPSO optimizer [58]. Despite the hypertuning costs, the accuracy benefit is high particularly in an exploration multidisciplinary optimization study of expensive analyses. Finally, if $e(\mathbf{x})$ is a smooth function — as in simple problems with accurate and robust LF tools — then RBF can be used to model it.

2.3. Surrogate based optimization modification to implement our Kriging approach

Our novel Kriging model implementation [54] not only improves the accuracy of the metamodeling approximation, but as a Gaussian approximation, it also allows the uncertainty estimation of the model itself [59,60] through the mean squared error (MSE). Combining the model prediction and its uncertainty allows the calculation of the EI [60], a metric expressing how much the function of interest is expected to improve in each design point. It depends on the current minimum point $y_{\min}$, the model prediction $\hat{y}$, the uncertainty $\hat{s}$ of the model itself, the cumulative distribution function Φ and the probability density function ϕ. The objective function of the SBO then becomes,

$$EI = (y_{\min} - \hat{y}(\mathbf{x}))\Phi\Big(\frac{y_{\min} - \hat{y}(\mathbf{x})}{\hat{s}(\mathbf{x})}\Big) + \hat{s}(\mathbf{x})\phi\Big(\frac{y_{\min} - \hat{y}(\mathbf{x})}{\hat{s}(\mathbf{x})}\Big) \tag{3}$$

To recover HF information in the EI estimation, the MSE of the error correction model $\hat{s_e^2}$ itself is also included. By superposition, the full MSE formulation is expressed:

$$\hat{s^2}(\mathbf{x}) = \sigma^2\Big[1 - \boldsymbol{\psi}^T\boldsymbol{\Psi}^{-1}\boldsymbol{\psi} + \frac{1 - \mathbf{1}^T\boldsymbol{\Psi}^{-1}\boldsymbol{\psi}}{\mathbf{1}^T\boldsymbol{\Psi}^{-1}\mathbf{1}}\Big] + \hat{s_e^2} \tag{4}$$

where σ^2, $\boldsymbol{\Psi}$ and $\boldsymbol{\psi}$ are the model variation, correlation matrix and vector respectively. Further details on the development of this MF Kriging correction (MF modKriging), are provided in Kontogiannis [54]. The optimization problem now reduces to maximizing the EI function during

the sub-optimization process. The introduced uncertainty information, gradually forces the method to unexplored regions, thus favouring a balance between pure local search and exploration — which is appropriate for the MDO conceptual design study considered in this work.

2.4. Multiobjective optimizer

The EI is a computationally cheap algebraic formulation allowing the use of a gradient free optimizer for the suboptimization process. Specifically, we apply our implementation of the Multiobjective Particle Swarm Optimization (MOPSO) [61,62] scheme that can efficiently provide a pareto front of new possible configurations. For a two-objectives optimization problem, the suboptimization process is formulated as,

$$\mathbf{x_1}^*, \mathbf{x_2}^*, \cdots, \mathbf{x_n}^* = \arg\left(\max_{\mathbf{x}\in D} \left(EI_1\right) vs \max_{\mathbf{x}\in D} \left(EI_2\right) \right) \tag{5}$$

Here, n pareto front candidates are identified in the design space D. This multiobjective approach also offers the advantage of parallel infill sampling, favouring load balancing that compensates for any potential expenses due to the MO search.

2.5. MF infill sampling approach

The error surrogate model $e(\mathbf{x})$ is also exploited in the infill stage, acting as a filter to avoid non-essential computational costs; design space points with low predicted error are analysed with the LF tool. Nevertheless, to ensure the introduction of HF information and thus the improvement of the design space and error space estimation, HF analyses are still imposed in a predefined iteration frequency. The optimization methodology is summarized in Fig. 1.

2.6. Constraints handling

Industrial applications demand understanding of the constraints and their handling methods, with both the final result and feasibility during convergence being desired. This discussion focuses on inequality constraints, but equality constraints can be transformed into inequality ones using tolerance parameters. In our methodology, in addition to the objective function, surrogate models of the constraints are also generated. Constraint satisfaction is forced during the suboptimization process with one of two methods: A hard *penalty* approach, in which a design point's EI value is set to zero if any of the constraint models predict a violation, steering the suboptimization towards feasible design space. Alternative forms of penalties are possible [56], but experience has showed that this approach is effective. The downside of this method is its dependency on the initial constraint surrogate accuracy. The second method is the *feasibility* approach, which requires a Kriging surrogate for the constraint function. By using the constraint limit instead of the current minimum value in the probability of improvement formulation, the probability of feasibility[2] (PF) [56] is defined. The simple suboptimization problem from eq. (6) now takes the form,

$$\mathbf{x}^* = \arg\left(\max_{\mathbf{x}\in D} PF \times EI \right) \tag{6}$$

For clarity a single objective case is presented here, but the concept is similarly applied in the multiobjective suboptimization problem presented in eq. (5). *Feasibility* uses information from the MSE of the model itself, enforcing the sampling of unexplored regions, improving its global accuracy. It has proven to be robust and effective, however it increases costs due to additional Kriging models. For more details on the behaviour of these methods, the reader is referred to Kontogiannis et al. [57,54]. More discussion on their implementation in this work is provided in section 4.2.

[2] Hereby, being simply called *Feasibility* for simplicity.

Table 1
Physical conditions for CRM case.

Condition	Value
Mach Number	0.85
Reynolds number	$2x10^7$
Pressure	23842 Pa
Temperature	220 K

Table 2
CRM V.15 Wing characteristics.

Parameter	Value
Span	52.64 m
Projected Area	167.95 m^2
MAC	3.19 m
Spars	2
Ribs	42
Range	17185 km[a]
Wingbox Structural mass	31000 kg

[a] This range corresponds to the clean wing. The respective range of the full CRM configuration is 13000 km.

3. CRM configuration model details

The CRM wing is a generic benchmark configuration [55] representing a typical supercritical transonic wing found in a widebody commercial transport aircraft. The geometrical and operational characteristics of the wing are shown in Table 1, 2. The model used in the present work is an up-scaling of the wind tunnel model, approximating real transport aircraft wing dimensions. Only the clean wing has been used in this study — the fuselage and engine nacelles have not been included in the model.

The outer mold line (OML) corresponds to a cruising (1g) shape and not the jig shape. Unfortunately, at the time this work was undertaken an actual jig shape CRM model was unavailable, with the cruising (1g) shape being the research standard. Therefore, both the OML and the structural model are being used as jig shape models.

For the structural analysis, the NASA CRM V.15 wingbox model is being used, as it features contemporary structural design elements used in such types of wingbox structures. Particularly, it features CBARs as implicit chord-spaced stiffeners and shear-webs instead of mid-chord spar to reduce computational cost and implicitly suppress local natural modes. In lieu of explicit stiffeners like stringers in the geometrical description of this model and given their importance in buckling loads, the thickness of the skin was increased simply to provide a more realistic starting geometry. The higher effective structural area is now acting as a longitudinal stiffener for bending loads. Apart from stress relieving, this prevents excessive displacements which in turn also accelerates the convergence of the multidisciplinary analysis loop.

Additional masses representing the slat and flap activation systems' have been included by CONM2 'lump masses' connected with RBE3 interpolation elements attached to the front and rear spar cap elements respectively. Three more lump COMP2 masses corresponding to fuel have been similarly included using three CONM2 elements, each one in the center of gravity of each fuel tank, as shown in Fig. 3(a).

With the fuselage not included in the wing design study, imposing the necessary cruise trim conditions requires defining a fixed fuselage, empennage and additional systems' weight along with the corresponding payload weight. The total take-off weight of the aircraft W_{TO} is calculated as follows:

$$W_{TO} = W_{w,str} + W_{fuel} + W_r \tag{7}$$

Here, W_r is a predefined operational empty weight statistically estimated based on the number of passengers, including weight kept constant during the optimization (payload weight, landing gear, wing movables, empennage, fuselage etc.). $W_{w,str}$ corresponds to the weight

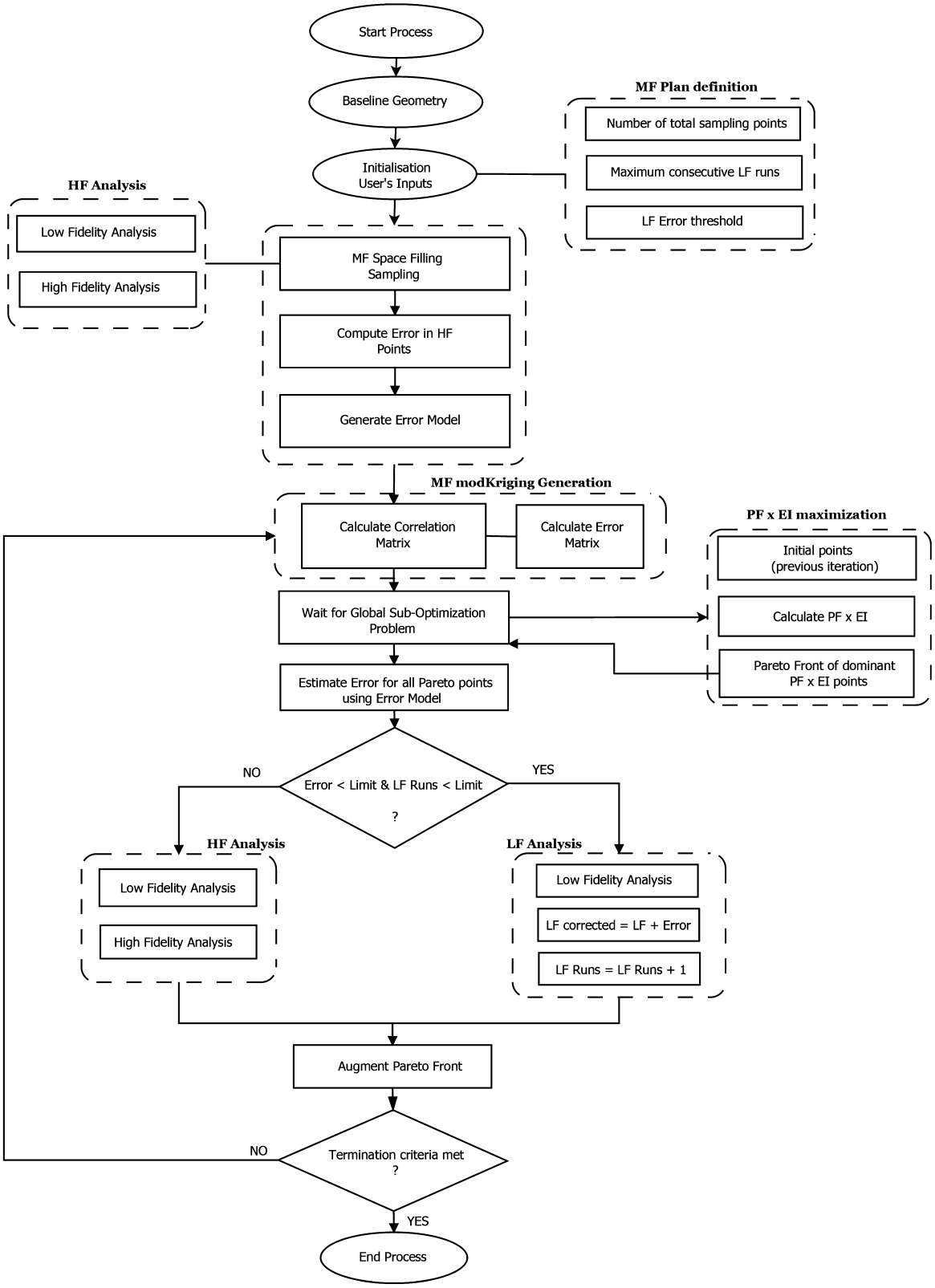


Fig. 1. Methodology used for the optimization of the CRM.

of the structural components of the wing provided by the NASTRAN code, and W_{fuel} is the weight of the fuel that can be stored within the wingbox. The fuel mass is calculated based on the internal volume of the wingbox, which in turn is dependent on the global design variables.

This weight estimation approach is hybrid, using Class I methods for the fuselage and the rest of the aircraft systems which are not included in the design optimization problem (W_r). The structural weight of the wingbox is estimated by the FEM model and as such it is a Class III weight estimation approach [63]. Using the take-off weight as an

objective function instead of mid-cruise weight is a technically sound decision since the range is also considered as a constraint. Hence, the optimization is not steered towards light but inefficient designs.

4. Optimization problem

4.1. Parameterization strategy

Conceptual studies typically examine the effect of small groups of well defined parameters and directions, up to basic shape design through inverse airfoil design. In the context of interest, the aerodynamic shape impacts the fuel tank capacity directly and the structural design efficiency through secondary moment of inertia effects. The global design parameters are controlled through a combination of Free Form Deformation (FFD) [64], accompanied by twist and sweep angle control. To the authors' experience, this strategy and the respective bounds are sufficient for a conceptual aerostructural study, and representative of the typical dimensionality of an early conceptual stage. Optimizing the aerodynamic shape is not the goal of this implementation, rather, exploring the fundamental mechanisms and design directions in a multidisciplinary problem conceptual study.

The FFD control points act directly on the grid, functioning as global design variables that alter the OML and the wingbox shape simultaneously. The bounds of the shape design variables represent the maximum X or Z displacement of any FFD control point, relative to the local chord. Sweep and twist are distinct variables controlled by a group of control points that move concurrently to achieve independent sweep/twist movement. No further parameterization steps are required to provide a ready for analysis computational model while the computational grid was ensured to be robust for such geometrical changes. The incidence angle is being used as an aerodynamic design variable to trim the configuration in cruise, since aerodynamic and structural design changes influence the total lift and weight of the wing. Although its presence is not mandatory from a mathematical perspective, it is a dominant — and essentially linear — factor from a physical sense. Relying solely on the rest of the variables for cruising, would introduce an additional requirement to shape design which is already loaded with the task of shock minimization. Structural parameters include the thickness of the wingbox elements: spars, shear-webs, ribs and skin [53]. In contrast to the MDF formulated problem [53], where structural elements were grouped, a structural sizing efficiently performed in the disciplinary optimization level, allows for a more detailed structural description. Each variable now corresponds to a unique structural element's shell thickness and the structural variables grouping described in the MDF formulation [53] is discarded. The aerodynamic and structural model parameterization is summarized in Table 3 and Figs. 2, 3(a) and 3(b).

4.2. Constraints

The cruising constraints required for the optimization to provide useful engineering feedback, take the following inequality form,

$$\frac{|L(\mathbf{x}) - W_{TO}(\mathbf{x})|}{W_{TO}(\mathbf{x})} \leq \epsilon \tag{8}$$

$$|C_{Mcg}(\mathbf{x})| \leq \epsilon \tag{9}$$

where L is the lift produced, C_{Mcg} is the moment coefficient around the center of gravity of the wing and the tolerance ϵ is set to $\epsilon = 0.05$. Longitudinal trim constraints (eq. (9)) are vital for the optimization of a final wing design. However, since the empennage and fuselage models are not available in this study, such a trim constraint becomes irrelevant and hence it is omitted.

Another constraint considered is range, estimated based on the aerodynamic as well as the weight performance of each design. Further to structural weight, it is dependent on the available fuel tank volume inside the wingbox, which is sensitive to the global design variables, hence, implicitly introducing a tank volume constraint. The fuel mass is directly calculated for every new developed design, and it is embedded in the structural model using CONM2 lump masses connected to spars and ribs through RBE3 rigid elements (distributed coupling multi point constraint). Three lump masses were used for three fuel tanks along the semi-span.

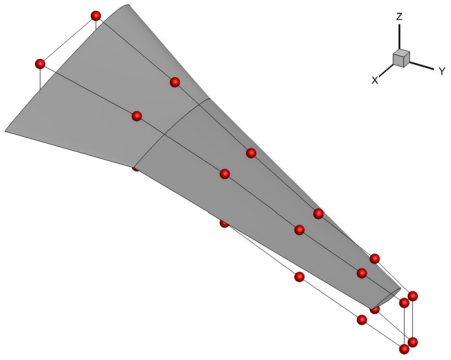


Fig. 2. FFD control points deforming the OML and the wingbox.

Table 3
Design variables.

Parameter	Count	Lower	Upper bound
Shape variables	20	-1 m	1 m
Spar thickness	Shell number	4 mm	21.1 mm
Rib thickness	Shell number	0.5 mm	7 mm
Skin thickness	Shell number	4.5 mm	19.5 mm
Sweep	1	33.5°	36.5°
Twist	1	-10°	10°
Angle of attack	1	2.8°	4°

The Range (R) is calculated using Breguet equation,

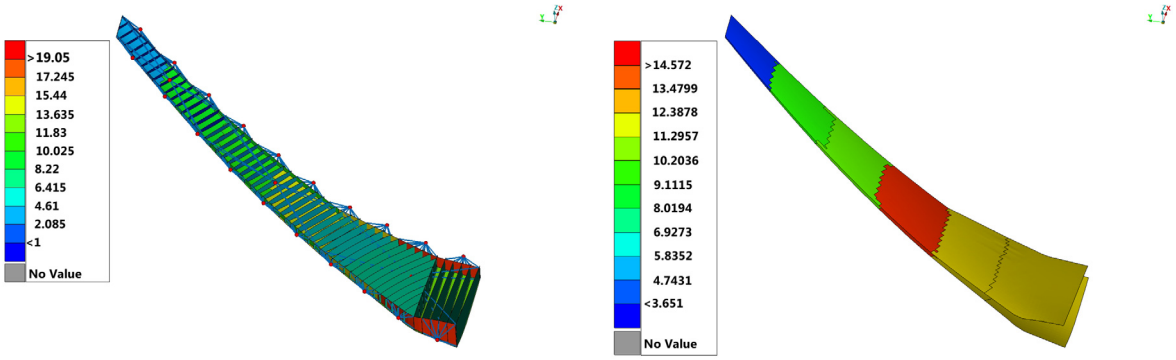
$$R(\mathbf{x}) = \frac{V}{gSFC}\frac{L}{D}\ln\left(\frac{W_i}{W_f}\right) \tag{10}$$

where V is the flight speed, SFC is the thrust-specific fuel consumption, W_i is the initial and W_f is the final weight.

To avoid an unrealistic and excessively flexible wing design, which would require a nonlinear structural analysis as well as being prone to flutter problems, we constrain the first bending mode frequency using the Nastran SOL103 for this modal analysis. This is a static analysis since dynamic aeroelastic effects or the impact of aeroelasticity on the control systems is outside of the scope of this MDO work. This constraint also ensures that the structural design will not be too local, since the eigenvalues are properties that depend on the whole structural wing design. A 2.5g maneuver was selected to ensure structural integrity. Although not an industrial standard limit load that would lead to a realistic wing design, this maneuver was defined to keep consistency with MDO literature. More details on the implementation of this constraint are provided on the structural sizing process overview in section 4.4.1. When the Feasibility method is used, the probability of feasibility of range PF_R, flight trim PF_{trim}, structural strength PF_{stress} and stiffness PF_{mode} are introduced in the suboptimization process which now becomes,

$$\mathbf{x_1}^*, \mathbf{x_2}^*, \cdots, \mathbf{x_n}^* = \arg\left(\max_{\mathbf{x}\in\mathbb{D}}\left(PF_R \times PF_{trim} \times PF_{stress} \times PF_{mode} \times EI_{C_D}\right) \; vs \max_{\mathbf{x}\in\mathbb{D}}\left(PF_R \times PF_{trim} \times PF_{stress} \times PF_{mode} \times EI_W\right)\right) \tag{11}$$

where the probability of feasibility for an inequality constraint problem of $g(\mathbf{x}) \leq g_c$ is expressed as,



(a) CONM2 masses represent fuel and high lift systems' masses, connected with the structure with RBE3 elements. For clarity, shear webs are omitted.

(b) Skin thickness variables and datum design thickness.

Fig. 3. CRM structural parameterization. Contours representing thickness that is in mm. (For interpretation of the colours in the figure(s), the reader is referred to the web version of this article.)

Table 4
Constraints.

Constraint	Value
Range (R)	$\geq R_{datum}$
Trim in Cruise ($trim$)	$\frac{\lvert L(\mathbf{x}) - W_{TO}(\mathbf{x})\rvert}{W_{TO}(\mathbf{x})} \leq \epsilon$
Von Mises ($stress$)	$\leq \sigma_y / SF$
1^{st} bending mode ($mode$)	$1 \leq f \leq 2\ Hz$

$$PF(\mathbf{x}) = \frac{1}{2}\left(1 + erf\left(\frac{g_c - g(\mathbf{x})}{\hat{s}(\mathbf{x})\sqrt{2}}\right)\right) \tag{12}$$

The constraints are summarized in Table 4.

4.3. Aerodynamic analysis

Two CFD analyses featuring different physics, grid and convergence tolerance are set up using the commercial solver ANSYS Fluent [65], to provide the global aerodynamic coefficients. The final result is averaged using values from the last 50 iterations to minimise noise induced by limited oscillation in the converged solution.

4.3.1. Low fidelity tool

Aiming in the minimization of computational expenses, the LF analyses neglect the effect of viscosity using specifically developed grids. Two candidates were examined in a mesh independence study, involving 10 and 15 structured layers respectively in a structured O-grid subdomain with the outer domain using unstructured mesh. The coarsest grid was chosen for its low cost and insignificant accuracy penalty. Additionally, to reduce costs further, we employed the concept of partial convergence [66]. In this, a maximum number of iterations is set after investigating the behaviour of the LF convergence [53] in various points in the design space. Thus, the LF error bounds are known. It should be said that the LF tool typically underestimates the drag force as well as the outboard load distribution [53]. Therefore, in the design space particularly associated with high geometric twist or/and low bending and torsional stiffness, the LF analysis is expected to provide increasingly false data.

4.3.2. High fidelity tool

The HF CFD analysis uses a Roe-FDS scheme [67], SA [68] to model turbulence effects and the equations are discretized with a 2^{nd} order upwind scheme. A hybrid grid was used (Fig. 5). The outer volume featured tetra elements while the subdomain was a structured O-grid. The subdomain ensured the required near wall resolution, defined following a grid convergence study [53] of four levels of successive refinement starting from $y^+ = 10$, to well within $y^+ = 1$, as illustrated in Fig. 4. Level 2 was selected as the most appropriate, showing satisfying physics resolution as well as converged aerodynamic coefficients. Both the LF and the HF mesh used volume mesh refinement techniques in the wingtip vortex region, as well as in the upper section area enclosing the predicted shockwave position. The boundary conditions were adjusted to define the problem as overviewed in Table 1, with pressure inlet and symmetry plane used to model the cruising conditions.

To demonstrate the difference between the LF and HF solution, the two pressure distributions (corresponding to the EULER and RANS analysis respectively) are provided in Fig. 6. It is evident that in the inner mid part of the wing, the two methods predict similar physical field. The location of the shock in the upper part of the wing near the root is almost identical for both cases, while in the middle of the wing it is located only slightly downwind of the one predicted by RANS, followed by a pressure fluctuation. In the same part as expected, the inviscid solution also underestimates the pressure losses. However, in the outer portion of the wing the models differ greatly. The inviscid analysis consistently predicts a more gradual pressure drop in the upper section of the wing — especially very close to the wingtip. As a result, the shock location is identified significantly further downstream of the one estimated by the RANS analysis. Furthermore, the effect of the increased geometric washout near the tip is pronounced in the inviscid solution. The upper LE section is a stagnation area from which the flow accelerates until the shock occurs in $x/c \approx 0.85$. In the lower side conversely, a sudden suction is predicted until the mid-chord location. This behaviour suggests an underestimation in the drag force predicted by the LF tool as well as wrong loads distribution in the outer part of the wing, effectively acting as loads alleviation.

4.4. Asymmetric subspace optimization architecture formulation

To keep this paper concise, our methodology is demonstrated only in an ASO environment. For MDF results, the interested reader is referred to [53]. The ASO architecture is well suited to poor load balancing problems as this case, where the structural analysis is significantly cheaper than any of the aerodynamic analyses. Furthermore, efficiency improvement comes from improved surrogate performance and more effective disciplinary optimization. More discussion on this can be found in [69].

The procedure followed by ASO architecture to tackle this aerostructural design problem is described in the XDSM diagram of Fig. 7.

4.4.1. Structural sizing

The structural sizing is the disciplinary optimization process aiming in minimizing the weight of the structure with respect to the local variables, in which case the thickness of the structural elements. The global variables dictating the wingbox shape design are constant dur-

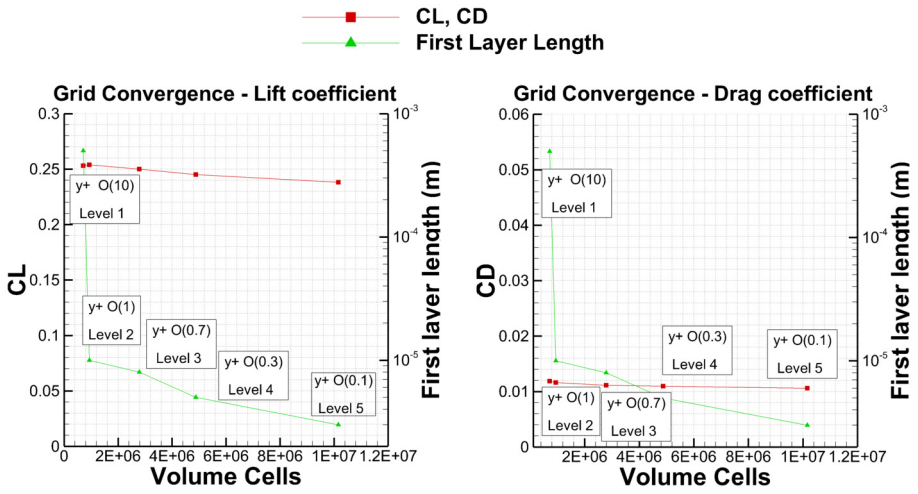


Fig. 4. Global aerodynamic coefficients grid convergence study for the HF analysis.

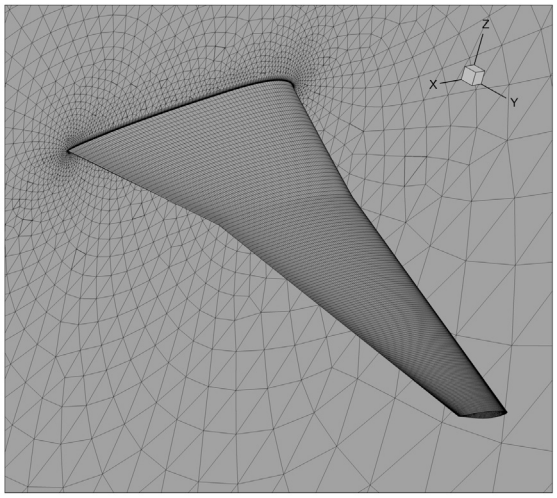


Fig. 5. High fidelity aerodynamic surface grid. O-type grid layers are used for boundary layer resolution.

ing this stage and are driven by the system level optimiser. The process is described as:

$$\min_{\mathbf{x_{str}} \in \mathbb{S}} W_{str}(\mathbf{x_{str}}) \quad \text{subject to } g_i(\mathbf{x}) = SF\frac{\sigma_i}{\sigma_y} - 1 \leq 0 \tag{13}$$

In Eq. (13), $\mathbb{S}$ is the structural design space where $\mathbb{S} \subset \mathbb{D}$, where $\mathbb{D}$ is the design space of both the global and structural variables. σ_i is the Von-Mises stress of the i^{th} element, and σ_y is the yield stress of the material, Aluminium 7050-T7451, with $\sigma_y = 469\,MPa$. SF is the safety factor, set to 1.5 and the loading corresponds to 2.5g.

The above procedure is performed by an efficient and dedicated MSC Nastran SOL200 process that uses gradient based methods as described in the work of Dababneh [70] and as such is robust against disciplinary dimensionality. The sizing process remains cheaper than a LF aerodynamic analysis as it uses the linear SOL101 static analysis; a reasonable assumption for the purposes of this study since the aspect ratio and wing deflections are not high [71,72]. Therefore, there would be no significant benefits in defining a lower fidelity structural analysis for the sizing process [73]. In fact, a wingbox analysis improves the accuracy of the LF aerostructural infill analyses, also making the weight metamodel — and the design space exploration — more efficient. A side benefit of using a single wingbox configuration is reduced complexity as we keep a single parameterization strategy.

4.4.2. A note on high loads maneuver structural analysis

There are few possible ways of simulating a high g maneuver. One would be to perform an aerodynamic analysis with an angle of attack corresponding to higher total lift than the cruising lift. This would be consistent with the load factor requirement, but it would provide a different load distribution. Although a topic rarely discussed in the literature, it is of great importance due to its impact in the optimization process. In our method, the high-g maneuver loading input of the structural analysis for the SOL200 sizing, is simulated by simply using a load factor of 2.5 in the aerodynamic loads of the current Gauss-Seidel iteration. A limitation of this work — as in our MDF formulation study [53] — is that the full aerostructural loop is not performed during the structural sizing, which simply uses the jig shape pressure loads as an input. Although not ideal, this reduces the analysis cost by almost 50%. It is a sensible approximation, given that the 2.5g maneuver aerodynamic load is also an approximation; actual maneuver loads would be resulting from a high angle of attack aerodynamic analysis.

Nevertheless, it should be noted that an accurate constraint function analysis is expected to increase the inwards shift of the aerodynamic load in high g conditions, due to high outboard structural deformation outboard acting as loads alleviation. Industrial experience suggests that information coming from a full maneuver aerostructural loop, would steer the optimization towards designs which during cruising conditions would feature a load distribution closer to the elliptic one.

4.5. Aerostructural loop: mapping the aero loads and structural displacements

Interdisciplinary communication between grid topologies in this loosely coupled analysis is being carried out with python scripts through the CAE software ANSA [74] using an RBF-based method [17]. Load transfer is done into two stages; mapping of the pressure loads corresponding to the wingbox skin area, and the loads from aerodynamic surfaces of no structural elements. The latter are the Leading Edge (LE) and Trailing Edge (TE) regions that are split into three LE/TE subsurfaces across the span. Pressure loads are integrated, defining a single resultant force acting on the respective center of pressure, which is connected to the respective structural beam elements using RBE3 elements. The process is shown in Fig. 8.

The structural displacements of the skin nodes are transferred to the jig shape aerodynamic surface mesh using RBF functions similar to Rendall and Allen's unified method [18]. Structural deformation is defined in an absolute manner, that is, as a difference between the aerodynamically loaded shape and the jig shape [53]. The aerodynamic volume mesh deformation is performed using an RBF method like the one described in the work by A. de Boer et al. [30].

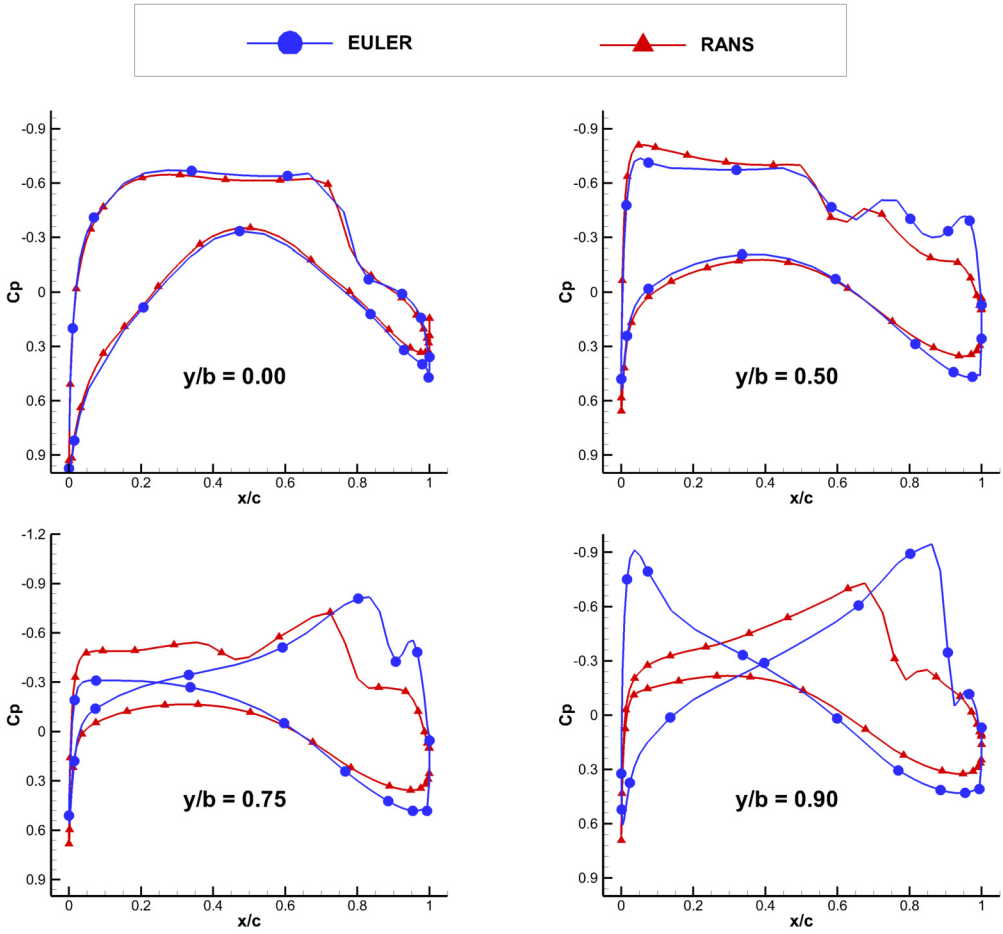


Fig. 6. Comparison between low fidelity (EULER) and high fidelity (RANS) solution in terms of pressure distribution.

5. Results

5.1. Sensitivity in constraint models

The MF EI methodology is very effective in exploring the design space and finding dominant designs since the effect of both global and disciplinary variables on the objective functions is significant. A concurrent drag and wingbox structural weight minimization is achieved in the first iterations after the sampling. Nevertheless, convergence is sensitive to constraint surrogate accuracy. The modal constraint is smooth so a cheap RBF model satisfies it in every infill point. However, cruising and range constraints are proven to be more challenging. Range includes the effect of fuel weight, structural weight and aero performance at the same time. The dependency on these quantities makes it highly nonlinear and multimodal, creating "islands of feasibility" within the design space. In a similar fashion, the cruising constraint space is filled with sparse regions of feasibility.

An explorative method like *Feasibility*, improves only the accuracy of the constraint surrogates in the initial iterations, before both feasible and promising solutions are identified in a high dimension space. On the other hand, the RBF based *Penalty* method is more aggressive, not investing infill data to constraint model improvement. Adding this to the poor accuracy of the cheap RBF metamodel in high dimensionality makes pareto front convergence challenging.[3] Shape parameters θ and θ_e selection becomes significant. If their values are below a critical level, the models become too flat so that information from the sparse sampling is diffused in the extrapolating regions of the design space. This creates fictitious promising points, steering the suboptimization process into false sampling points in or near the bounds. Consequently, improving the knowledge of the actual promising design space regions is prevented, stalling the optimization process completely.

The above problem is not a showstopper in an exploitation optimization scheme [75], where the process is initiated from the datum area. In this, constraint values are locally available and cheap RBF models are reasonably accurate. However, we do not use this approach as it does not satisfy the exploration requirements of a conceptual study, on top of involving a prohibitive number of direct LF analyses.

The physical correlation between lift and structural weight, also identified through parallel coordinates, impacts the cruising constraints' satisfaction. Reducing the wing's thickness through global variables, reduces both drag and structural weight penalising the fuel mass capacity. Subsequently, to satisfy range, an increase in L/D is required but the optimizer is also trying to steer to $L = W$ solutions. Therefore, the accuracy of the cruising constraint is critical for the satisfaction of range. When RBF based Penalty method is used, it leads to thin, low weight, low fuel solutions of insufficient lift and L/D to satisfy range. The *Feasibility* method is inherently more conservative than Penalty, while also using the more accurate Kriging model — tuning the error model shape parameters is critical to correct the LF metamodels. It tackles the problem of steering towards fictitious promising configurations in the extrapolating regions, with convergence gains justifying its use over the cheaper RBF/Penalty option.

[3] For more information on the convergence behaviour of *Penalty* and *Feasibility* methods, see Kontogiannis et al. [57].

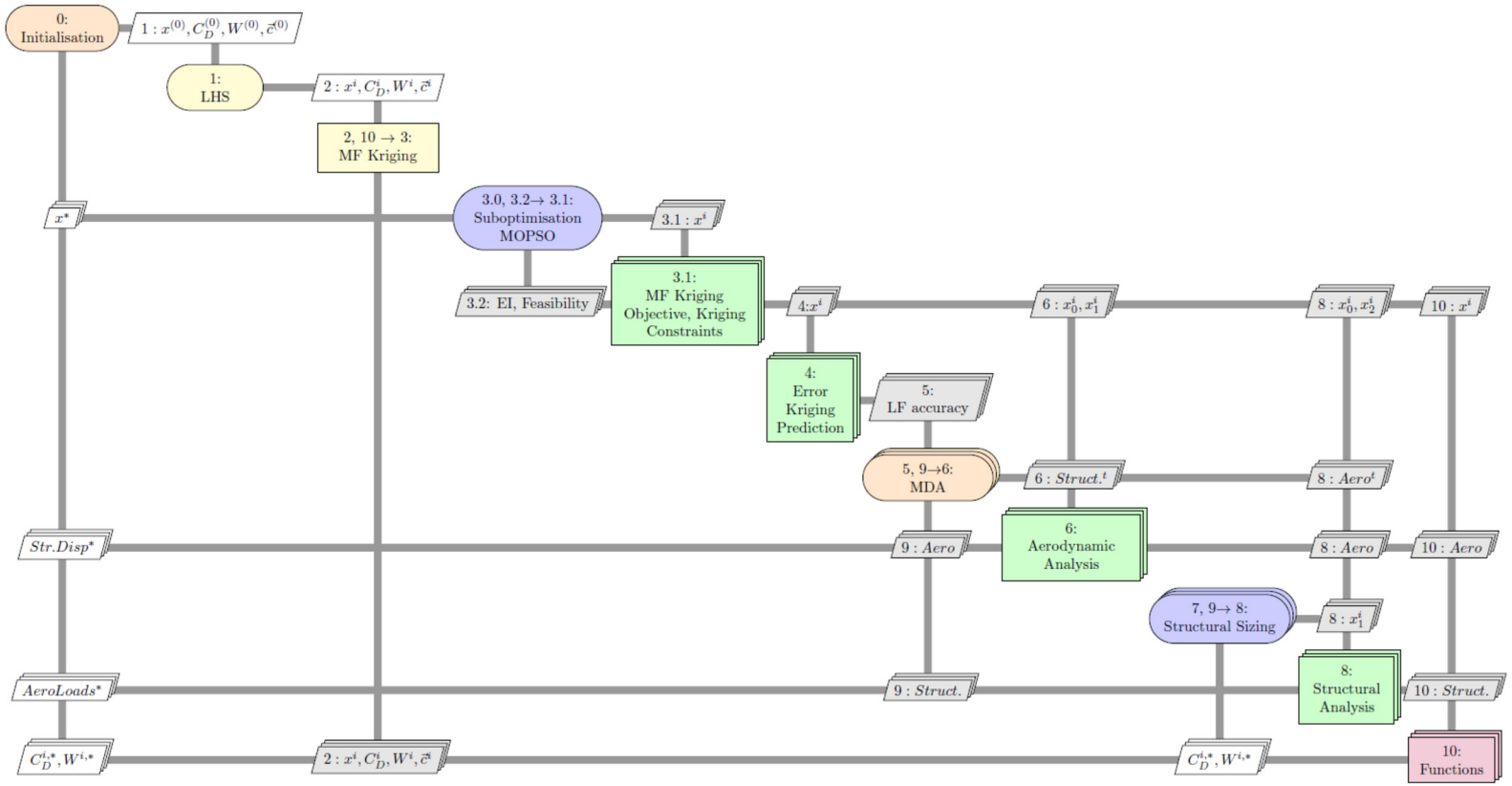


Fig. 7. XDSM flowchart for ASO formulation of CRM aerostructural optimization.

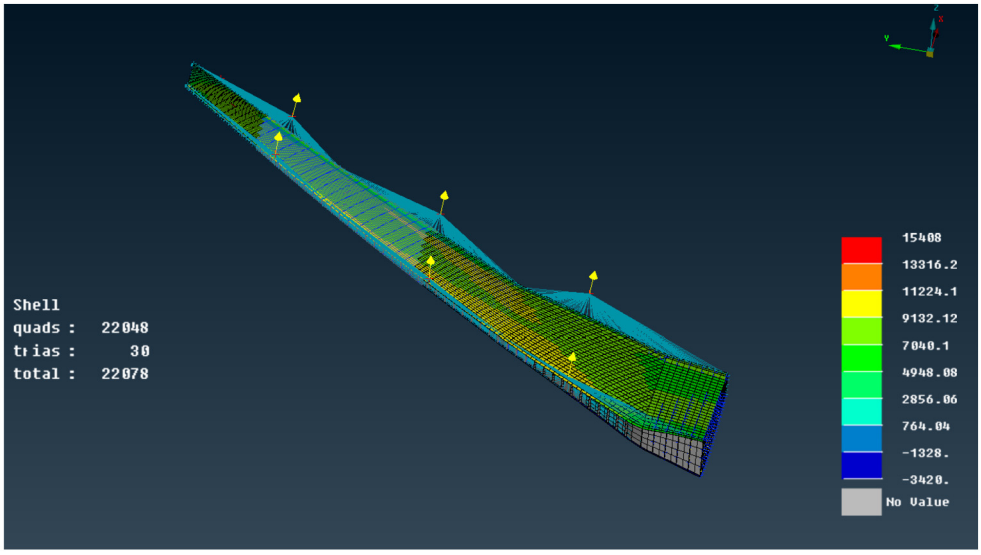


Fig. 8. Aerodynamic loads mapping: Pressure loads are interpolated with RBF functions, while LE/TE forces are transferred to the beams using RBE3 elements.

5.2. Pareto front results

Due to the above, the *Feasibility* method with Kriging metamodels had to be used. Despite system level dimensionality in ASO being lower than in MDF [53], RBF was still not effective in satisfying the error correction of cruising constraint ($L = W$). Partly, this comes from the limited accuracy of RBF models, and partly from the challenging nature of this constraint specifically within the ASO formulation.

The cruising constraint metamodel predictor y correlates $L - W$ with the global variables (wingbox design), $y : y(W_{str}) = y\big(W_{str}(x_0)\big)$. However, a part of the physical mechanism responsible for the structural weight value is expressed through the local variables, $y : y(W_{str}) = y\big(W_{str}(x_0, x_{str})\big)$. The *lack of the explicit* description of the effect of the local variables on the constraint metamodel, raises an *implicit mapping* between the global and the local variables when estimating the cruising condition. This is because a global variables set corresponds to a local one in a deterministic way, through the *gradient based* structural sizing process. That is, $x_0 \rightarrow x_{str}$; which makes the model $y : y(W_{str}) = y\Big(W_{str}(x_0(x_{str}))\Big)$.

In Fig. 9, we provide a comparison between a standard HF EI and our MF EI approach for a given computational budget — that is predefined wall time. Both pareto front extents are similar, with the MF designs dominating most of the HF ones, hence our methodology succeeds into improving the pareto front over the equivalent HF method for the same wall time cost. This result supports our claims regarding the usefulness of our multifidelity methodology, particularly in conceptual multiobjective studies, since: it accelerates the initial design exploration, reaching promising directions but using multifidelity information in an appropriate way. It is a rapid conceptual tool leading to designs more mature than a typical LF and HF study do in a given wall time. After that MF exploration phase, the MF pareto an function as a starting point for parallel HF local (e.g. adjoint based) optimization studies.

The HF EI approach is more beneficial on the low weight objective space and provides more points. Furthermore, both methods propose configurations of similar structural weight. This suggests the existence of (at least) three strong local minima in the structural weight design space, forming three (at least) efficient design trends. Interestingly, a reduction in aerodynamic performance is observed in MF pareto front points showing interdisciplinary synergy through disciplinary tradeoff. The pareto front sets are generated when none of the conflicting disciplines is optimized, and as in the MDF case [53], the maximum range

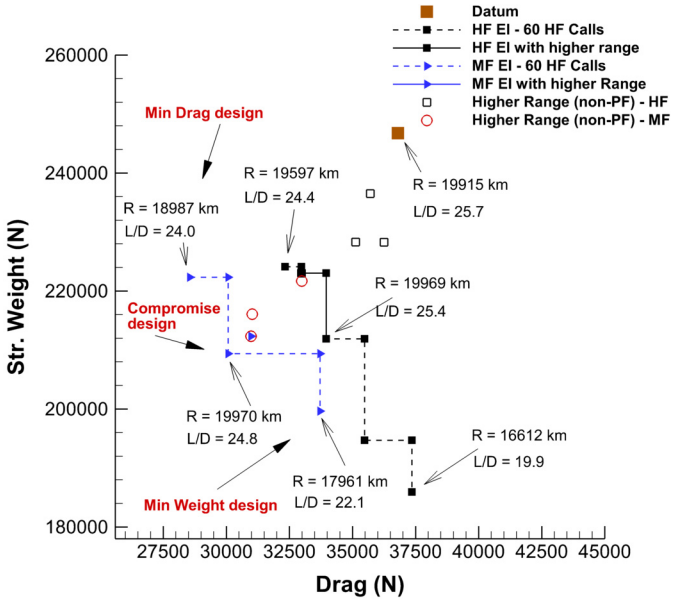


Fig. 9. Pareto front comparison between the HF and the MF methods, using *Feasibility* to handle the constraints for the ASO formulation. As in MDF, a tradeoff is required between aerodynamics and structures to achieve range performance.

performance occurs in the tradeoff pareto point.[4] This underlines the importance of multidisciplinary design processes, in this case structural design should not be overlooked in favour of aerodynamics. Also, since the range achieved by the MF and the HF tradeoff point are almost identical, the effect of interdisciplinary synergy on the design trends is once again obvious. The MF design achieves the same range performance, but with a lower drag value resulting from lower lift requirements, which in turn is the result of a slightly lower structural weight.

The MF method shows a lack of robustness and consistency in dominating the HF one, especially in such complicated multiobjective prob-

[4] Notice also that the range value shown on the datum point of this figure is higher than the one reported in Table 2. This is the result of the structural sizing.

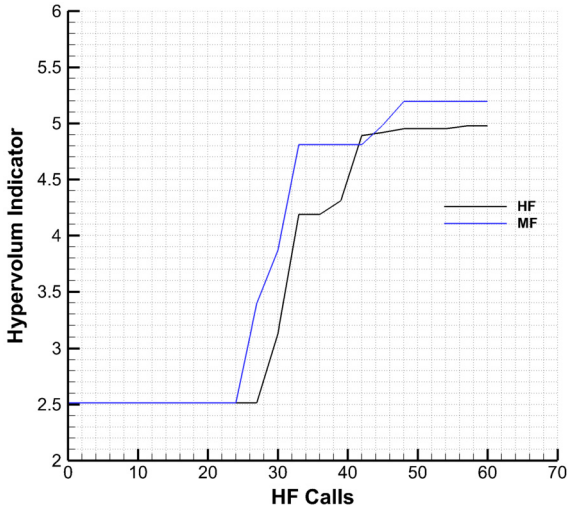


Fig. 10. Comparison between HF and MF convergence via the hypervolume indicator.

lems as also observed in our recent work [62], discussing single and multiobjective cases. Therefore, in Fig. 10 we are using the hypervolume indicator to provide information regarding the evolution of the HF and MF pareto fronts.

Evidently, the MF method is superior to HF in the early stages of the optimization process, fullfilling its original target — bring HF information earlier in the design stage. It later forms more extended convergence plateaus, attributes also observed in our single objective applications of the RAE2822 test case [62]. The plateaus towards the end of the optimization process suggest that the HF EI could be more efficient from that point on in the process; an observation consistent with the typical design process workflow, which uses LF tools in early stages and HF tools in later ones.

As a final note, LF tool cost should not be neglected when assessing MF methodologies. In this particular case, the cost of a LF analysis never exceeded a 30% of the HF one, and performing LF and HF analyses on parallel allowed an almost identical elapsed time cost between the two approaches. Finally, considering that the LF tool used in this work is accurate and robust (being an Euler CFD/SOL101-SOL200 analysis loop), only a tool of similar accuracy and robustness but of lower cost would be able to improve the presented results in terms of multifidelity efficiency.

5.3. Physical interpretation

The physical and design characteristics of the pareto configurations are discussed since they represent the information that would be exploited by the design engineers. In that sense, the structural stiffness and efficiency of the minimum drag, compromise and minimum weight design are examined based on the vertical displacements and Von Mises stress distribution respectively.

Fig. 11 displays the Von Mises stresses in the structural elements of the datum and pareto configurations. For each wingbox design — controlled by the global variables — the structural design is optimized. Stuctural optimization leads to the maximum allowed stresses to provide the minimum structural weight [76]. Peak Von Mises stress is maximised in every wingbox configuration regardless of the corresponding design direction (be it minimum drag or minimum weight). Contrariwise to the MDF cases [53], this maximum stress is constant throughout the skin and is of course the maximum yield stress allowed based on the defined safety factor, showing the efficiency of the structural sizing process.

Stiffness characteristics are to an extent dependent on the thickness of the structural elements, and since structural thickness is optimized for all the configurations, the vertical displacements during a 2.5g maneuver are similar in all design approaches (as shown in Table 5). This is in contrast to MDF [53] where the structural design was not as efficient for all the pareto configurations depending on aerodynamics or structural orientation. The structural sizing efficiently leads all directions to the minimum allowed structural element thickness and the design direction is mainly a result of the global variables,[5] control of the Outer Mold Line (aerodynamic performance) and wingbox shape (fuel tanks volume and structural mass). The local variables (structural element thickness) also affect the fuel tank volume, but this is neglected as not leading to significant volume difference and since within SOL200 shell elements are not associated with a physical volume.

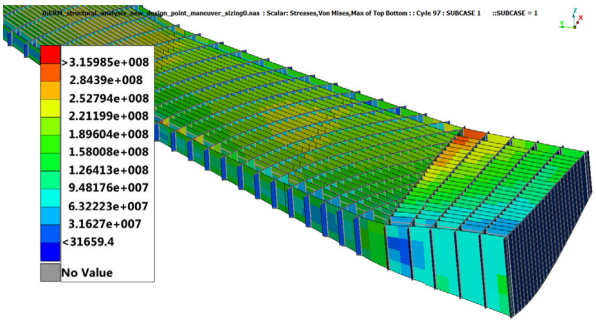
Table 5, reports the maximum stresses, tip displacements and skin thickness of each pareto direction. Skin thickness is reduced towards the tip with a local thickness increase near the Yehudi break (detailed panel thickness provided in [69]), which is the most critical region, guiding the structural sizing process to slightly higher local thickness values than in the actual wing root. The skin panel elements are thicker in the ASO than in the MDF formulation [53] since structural sizing is undoubtedly more efficient than the MDF structural design. The skin panels function implicitly as spar caps as well, providing “effective spar cap area”, maximizing the second moment of inertia so that the Von Mises stress constraints are met. Non critical regions like shear webs that are closer to the neutral axis, are significantly thinner. The same also holds for the ribs, which do not have to be as thick as the skin and the front/rear spars that also take torsional loads. This detailed and more effective structural design is the key advantage of the ASO over the MDF formulation.

The (jig) sweep for all design directions is also provided in Table 5. In this formulation case, characterized by the limited number of system level variables, all pareto front configurations show minimal deviation from datum.

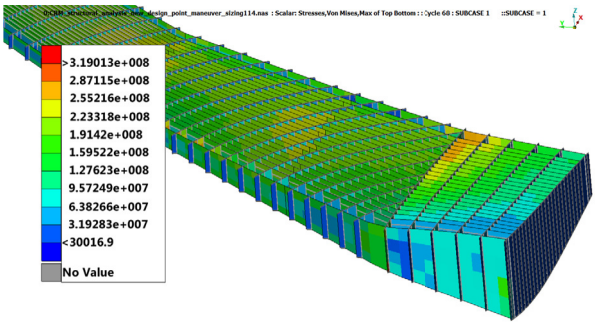
Fig. 12 displays the aerodynamic characteristics of the pareto configurations. Transonic aerodynamic design efficiency primarily comes by shaping the upper surface so that suction peak is achieved gradually, reducing wave drag losses. The pressure side is fairly similar for all configurations, resembling and maintaining a typical supercritical shape especially towards the outer part of the span. In fact, Fig. 12 in $y/b = 0.90$, imply that aerodynamic performance inefficiencies such as the strong suction peak in the lower section (particularly in the compromise and minimum weight designs), are due to higher structural deformation (especially torsional) which increases the washout — accelerating the flow locally in the lower leading edge section; not the airfoil shape itself. Near the root, which is less affected by structural displacements, the upper sections are similar as the main drag reduction mechanism has been identified. The pressure is decreased gradually until it reaches the critical Cp value followed by a shock wave of reduced intensity. Up to mid span the compromise and minimum weight design still experience strong shocks, whereas the outer span is more efficiently designed, with the compromise configuration sharing an almost identical upper section Cp distribution with the minimum drag configuration.

The torsional deformation of the ASO configurations (Fig. 12(b)) is higher than the stiffer MDF-based one [53], and even the minimum weight configuration has a reasonably efficient strong shock-free airfoil shape (something not observed in the MDF formulation). Evidently, the reduced system level dimensionality in ASO was beneficial for the aerodynamics discipline, as the surrogate models were more accurate.

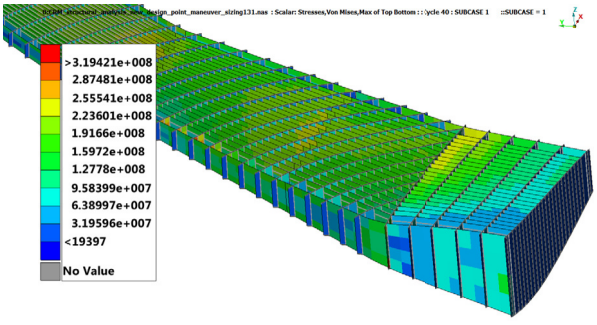
[5] Of course the local variables have an effect as well since the potential of thickness/weight reduction during the structural sizing is not constant throughout the system level design space.



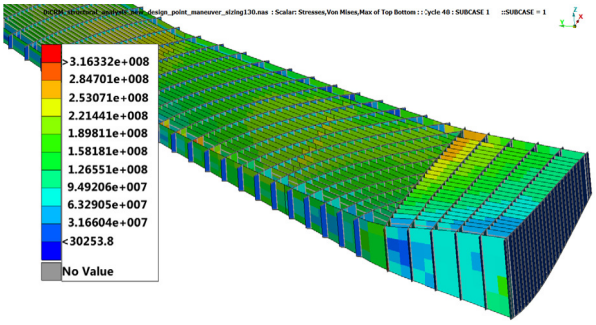
(a) Datum, max Von Mises stress: 315 MPa



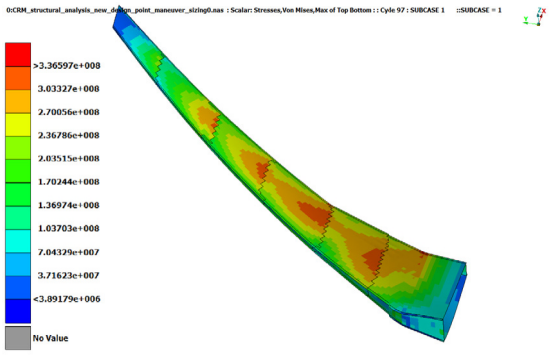
(b) Minimum Drag design, max Von Mises stress: 319 MPa



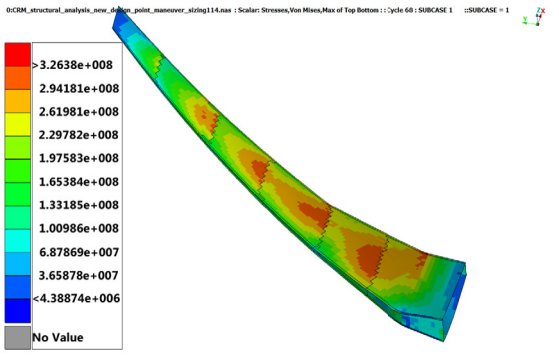
(c) Compromise design, max Von Mises stress: 319 MPa



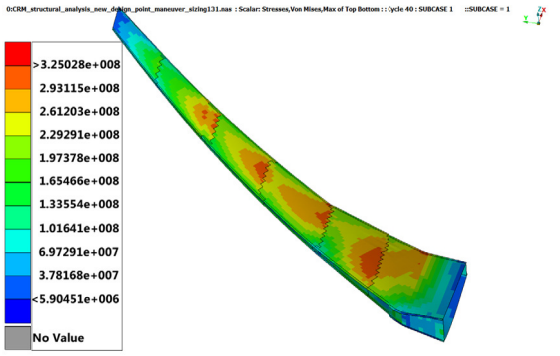
(d) Minimum Weight design, max Von Mises stress: 316 MPa



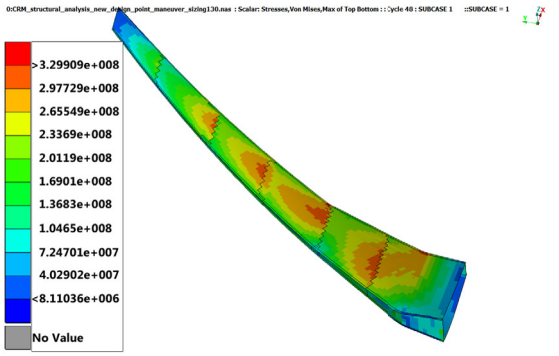
(e) Datum, max Von Mises stress: 315 MPa



(f) Minimum Drag design, max Von Mises stress: 319 MPa



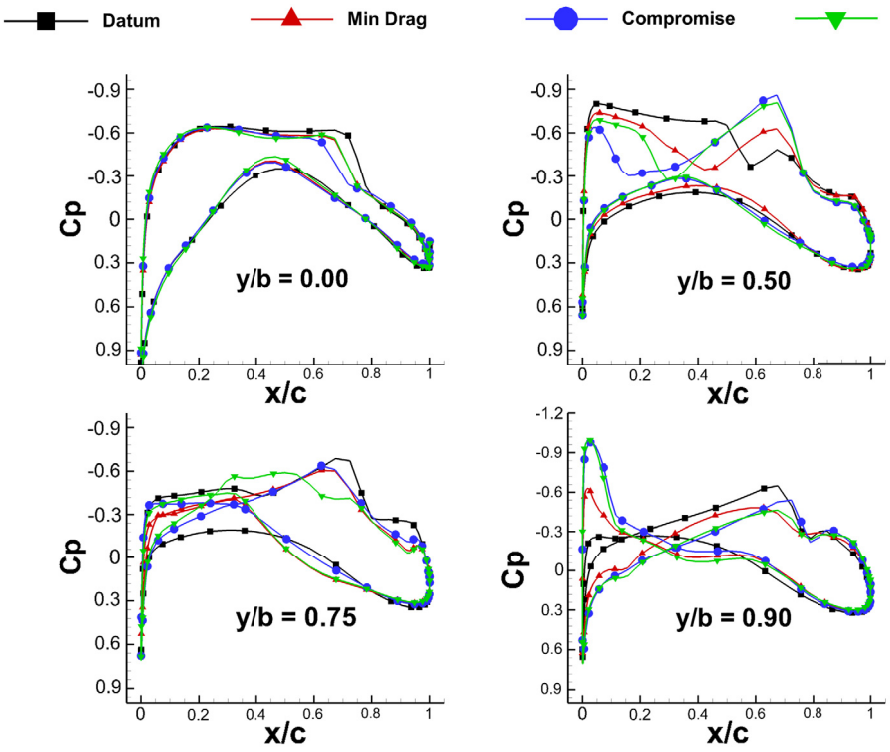
(g) Compromise design, max Von Mises stress: 319 MPa



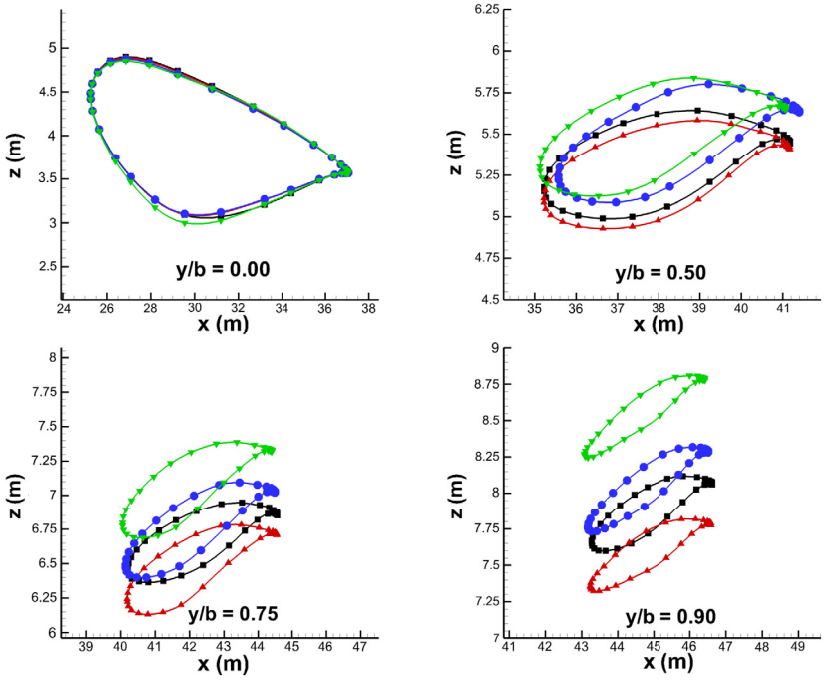
(h) Minimum Weight design, max Von Mises stress: 316 MPa

Fig. 11. Maximum Von Mises stress in the rib-shear webs and skins during high g maneuvers, (MPa).

Although all designs display similar vertical displacements on the 2.5g maneuver condition, their respective bending deformations differ during cruising conditions (evident from Fig. 12(b) as well). This trend is similar to the one observed in the MDF formulation [53], in which the minimum drag configuration was the stiffest with the minimum weight design experiencing the maximum displacements. This suggests



(a) Pressure distribution in different locations across the span.



(b) Wing sections in different locations across the span.

Fig. 12. Aerodynamic characteristics of the datum, minimum drag and compromised design.

that away from the sizing conditions, the structural behaviour is more dependent on wingbox than elements' thickness. In optimization terms, the global variables (through system level) are exploring the multiobjective problem, while the local variables are important for the satisfaction of the (structural) constraints. This is why during the cruise conditions that provide the objective function values, the proposed system level optimization framework behaves as expected, confirming its multiobjective exploration attributes.

5.4. Comparison between the formulations

We provide further comparison between MDF and ASO results, with respect to their pareto front solution as well as further physical in-

Table 5
Maximum Von Mises stress, tip displacement during high g maneuver, maximum skin thickness and jig shape aerodynamic sweep for each design direction.

Design Direction	Max Von Mises (MPa)	Tip Displacement (m)	Max Skin Thickness (mm)	Jig Sweep (deg)
Datum	315	5.2	18.5	35
Minimum Drag	319	5.1	16.1	34.98
Compromise	316	4.9	17.3	34.86
Minimum Weight	316	4.9	15.2	34.57

sight in the form of lift distribution. The objective space exploration characteristics are of course also dependent on the multifidelity formulation and the surrogate based optimization plan but, here the effect of the architecture alone is discussed. Regarding the pareto front, a lack of objective space exploration was observed in the case of ASO architecture. This trend is evident in Fig. 13 and it is attributed to two factors associated with the MDO architecture: Firstly, the reduction of the global variable design space leads to an objective space reduction and less diverge designs. However, more significant is the effect of the structural sizing which allows for better exploitation for each main design direction (dictated by the global variables). For each global design point, the disciplinary optimization focuses on only one of the objectives, not promoting objective exploration — hence MDF displaying wider pareto fronts than ASO. On this case, the structural sizing produces the minimum possible weight design and the overall performance is implicitly improved. The drastic weight decrease leads to drag savings through interdisciplinary coupling and lift constraints; an effect not fully exploited in its full potential by MDF due its higher dimensionality. Therefore, the narrower pareto front is a consequence of a more efficient optimization formulation, evident by the qualitative comparison of Fig. 14. Drag exploration is mainly affected by the global variables' exploration which is inherently more challenging due to heavier analyses (aerodynamics) leading to fewer loops (local iterations $\gg$ global iterations). As such, the weight reduction is more mature than drag reduction.

Although qualitatively similar, the ASO case displays greater improvement with respect to its initial value. The reduced system level dimensionality in ASO makes the metamodels more efficient, while requiring fewer HF analyses during the initial sampling. Since their datum points performance is not identical (because of structural sizing acting also in the datum in the ASO formulation), the curves should be compared only in a qualitative manner.

Nevertheless, Fig. 13 illustrates the superiority of ASO over MDF in terms of final values and range performance. The most significant improvement comes from the introduction of structural sizing which consistently reduces the structural weight. Furthermore, a small observed drag decrease is a result of more efficient surrogate modelling that comes with lower dimensionality. There is also a secondary interdisciplinary effect between aerodynamics and structures. With decreasing weight, the required cruise lift is also reduced. Therefore, lower lift allows for decreased wave drag (and induced drag as well). It should be mentioned though, that the drag reduction is not sufficient to maintain the same level of L/D as in the MDF cases. An MDO architecture involving an aerodynamics disciplinary optimization might be able to maintain or even improve L/D levels. Nevertheless, despite this decrease in aerodynamic efficiency, the range is increased due to the structure weight reduction (see Breguet equation in Eq. (10)). Typical range increase is in the order of $6\% - 14\%$ between analogous pareto points, with the highest range achieved by the tradeoff in both architectures. These two points show the importance of interdisciplinary synergies and MDO for efficient aircraft design.

Another way to view the multidisciplinary approach against an aerodynamics-led approach is through the normalized spanwise lift distribution (normalization against maximum sectional lift) (Fig. 15). In that sense, the datum lift distribution is compared against the distribution used by the tradeoff design of each MDO approach. The findings

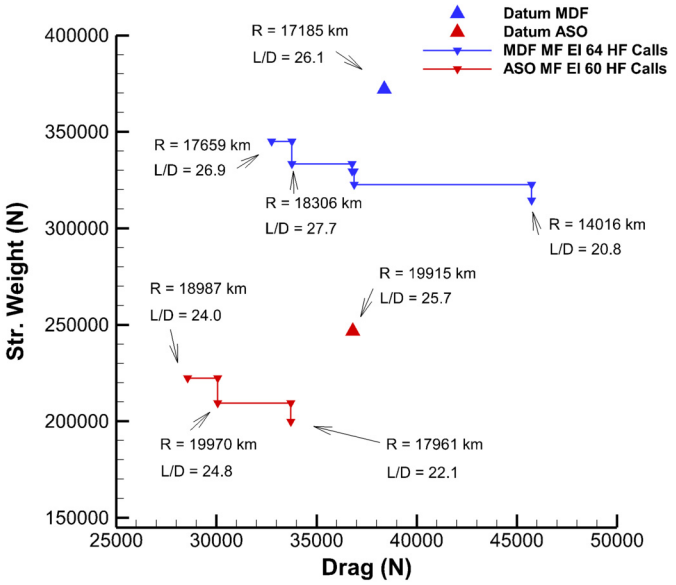


Fig. 13. Comparison between the pareto front generated using the MDF and the ASO formulation.

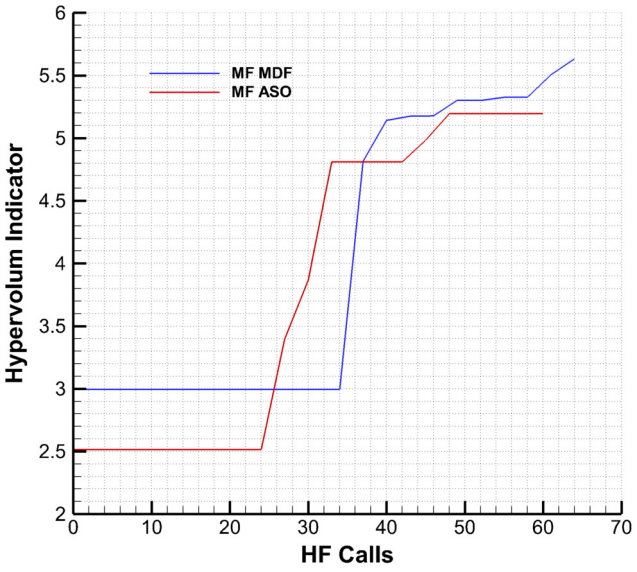


Fig. 14. Comparison between the convergence of pareto front generated using the MDF and the ASO formulation using the hypervolume indicator.

are in agreement with the conclusions of other researchers [77], since the MDO-based configurations lead to an inwards loading shift pattern. Shifting the aerodynamic load towards the root allows for a lighter structure. As shown by various researchers, as well as in Fig. 9, the efficiency of the complete aircraft system (e.g. range) is maximized when both disciplines interact beneficially, not when one of these is opti-

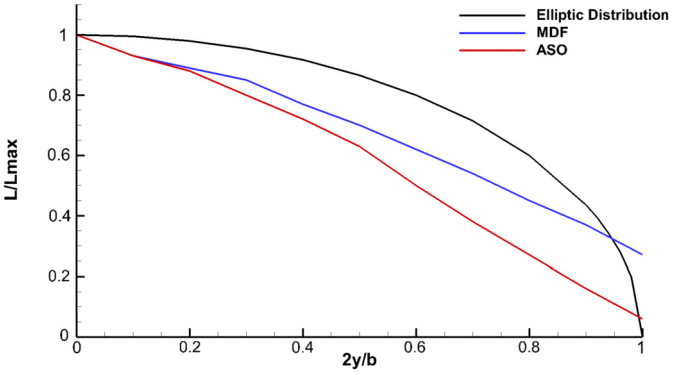


Fig. 15. Comparison between the normalized lift distribution resulting from the MDF and ASO formulations and that of the aerodynamic optimum.

mized. In this sense, although the MDF/ASO lift distributions do not correspond to an aerodynamic optimum, the structural gains they allow make the overall design superior. Finally, it was expected that ASO — being a more structurally efficient approach would follow a more aggressive inward load shifting direction than MDF. The system level guides the multidisciplinary process towards inboard-loaded designs, so that the disciplinary optimization can maximise the structure weight reduction, which eventually is what makes ASO configurations superior to MDF ones.

6. Conclusions

A shift to a multidisciplinary design process is the required next step the aerospace industry needs to take towards improving the efficiency of future aircraft configurations. However, interdisciplinary synergies should be exploited early in the design stage, where a wide design space is still available for exploration. In this work, to perform fast and reliable conceptual multidisciplinary optimization, our multiobjective multifidelity surrogate based optimization framework was applied within the asymmetric subspace optimization architecture. Our test case featured the Common Research Model, including the detailed wingbox model, representing a typical industrial aerostructural wing design application. Hence, we demonstrate how our methodology and this particular architecture can be used for a complex industrially relevant problem. The range and particularly cruising constraints proved to be very sensitive and challenging, requiring the use of more expensive but conservative constraint handling approach that involved a Kriging error correction model. The results highlight the necessity of interdisciplinary studies and the advantage of multifidelity tools in the early stage of the optimization process. However, despite favourable early convergence characteristics, multifidelity benefits gradually fade towards the later stages of the process. The major drawbacks include the sensitivity of the method's performance to the low fidelity tool itself and the seemingly superiority of the high fidelity results in the follow up detailed stages. Studying the impact of the multidisciplinary formulation itself, the asymmetric subspace optimization architecture confirmed to be a noteworthy improvement over the multidisciplinary feasible approach in every aspect. This was due to the increased efficiency of the lower dimensionality system level optimization, as well as the significant structural weight reductions achieved through the structural sizing disciplinary optimization process.

CRediT authorship contribution statement

Spyridon G. Kontogiannis: Writing – review & editing, Writing – original draft, Visualization, Validation, Supervision, Project administration, Methodology, Investigation, Formal analysis, Data curation, Conceptualization. **A. Mark Savill:** Supervision, Resources, Project administration, Funding acquisition. **Vasileios Mazis:** Resources, Methodology. **Vangelis Skaperdas:** Resources, Methodology.

Declaration of competing interest

The authors declare the following financial interests/personal relationships which may be considered as potential competing interests: Spyidon G. Kontogiannis reports financial support was provided by Innovate UK. If there are other authors, they declare that they have no known competing financial interests or personal relationships that could have appeared to influence the work reported in this paper.

Data availability

The data that has been used is confidential.

Acknowledgements

This project was co-funded by Innovate UK as part of the ATI Agile Wing Integration Project, led by Airbus and iCASE PhD award from EPSCR/Airbus.

References

[1] T.F. Wunderlich, Multidisciplinary wing optimization of commercial aircraft with consideration of static aeroelasticity, CEAS Aeronaut. J. 6 (3) (2015) 407–427, https://doi.org/10.1007/s13272-015-151-6.
[2] Q. Liu, M. Jrad, S.B. Mulani, R.K. Kapania, Integrated global wing and local panel optimization of aircraft wing, in: 56th AIAA/ASCE/AHS/ASC Structural Dynamics, and Materials Conference, 2015, AIAA 2015-0137.
[3] S. Doyle, J. Robinson, V. Ho, G. Ogawa, M. Baker, Aeroelastic optimization of wing structure using curvilinear spars, ribs (SpaRibs), in: 58th AIAA/ASCE/AHS/ASC Structures, Structural Dynamics, and Materials Conference, 2017, AIAA 2017-1303.
[4] G.J. Kennedy, G.W. Kenway, J.R.R.A. Martins, High aspect ratio wing design: optimal aerostructural tradeoffs for the next generation of materials, in: 52nd Aerospace Sciences Meeting, AIAA SciTech Forum, 2014, AIAA 2014-0596.
[5] C. Anhalt, H.P. Monner, E. Breitbach, Interdisciplinary Wing Design – Structural Aspects, 03WAC-29, German Aerospace Center (DLR), Institute of Structural Mechanics, 2003, https://doi.org/10.4271/2003-01-3026.
[6] N. Bons, J.R.R.A. Martins, Aerostructural wing design exploration with multidisciplinary design optimization, in: 58th AIAA Aerospace Sciences Meeting, AIAA Scitech Forum 2020, Orlando, 2020, AIAA paper 2020-0544.
[7] I.R. Chittick, J.R.R.A. Martins, An asymmetric suboptimization approach to aerostructural optimization, Optim. Eng. 10 (1) (2009) 133–152, https://doi.org/10.1007/s11081-008-9046-2.
[8] N.D. Polyzos, S. Vouros, I. Goulos, V. Pachidis, Multi-disciplinary optimization of variable rotor speed and active blade twist rotorcraft: trade-off between noise and emissions, Aerosp. Sci. Technol. 107 (12) (2020), https://doi.org/10.1016/j.ast.2020.106356.
[9] H. Zhang, B. Song, F. Li, J. Xuan, Multidisciplinary design optimization of an electric propulsion system of a hybrid UAV considering wind disturbance rejection capability in the quadrotor mode, Aerosp. Sci. Technol. 110 (3) (2021), https://doi.org/10.1016/j.ast.2020.106372.
[10] S.A. Brown, Displacement extrapolation for CFD+CSM aeroelastic analysis, in: 38th Structures, Structural Dynamics, and Materials Conference, Structures, Structural Dynamics, and Materials and Co-Located Conferences, 1997, AIAA Paper 1997-1090.
[11] P. Thevenza, T. Blu, M. Unser, Interpolation revisited, IEEE Trans. Med. Imaging 19 (7) (2000) 739–758, https://doi.org/10.1109/42.875199.
[12] C. Farhat, M. Lesoinne, P. Tallec, Load and motion transfer algorithms for fluid/structure interaction problems with non-matching discrete interfaces: momentum and energy conservation, optimal discretization and application to aeroelasticity, Comput. Methods Appl. Mech. Eng. 157 (1–2) (1998) 95–114, https://doi.org/10.1016/S0045-7825(97)00216-8.
[13] J.R. Cebral, R. Lohner, Conservative load projection and tracking for fluid-structure problems, AIAA J. 35 (4) (1997) 687–692, https://doi.org/10.2514/2.158.
[14] R. Lohner, C. Yang, J. Cebral, J.D. Baum, H. Luo, D. Pelessone, C. Charman, Fluid-structure interaction using a loose coupling algorithm and adaptive unstructured grids, in: M. Hafez, K. Oshima (Eds.), Computational Fluid Dynamics Review, John-Wiley, 1995.
[15] M.J. Smith, C.E.S. Cesnik, D.H. Hodges, Evaluation of some data transfer algorithms for noncontiguous meshes, J. Aerosp. Eng. 13 (2) (2000) 52–58.
[16] M.J. Smith, D.H. Hodges, C.E.S. Cesnkik, Evaluation of computational algorithms suitable for fluid-structure interactions, J. Aircr. 37 (2) (2000) 282–294, https://doi.org/10.2514/2.2592.

[17] A. Beckert, H. Wendland, Multivariate interpolation for fluid-structure-interaction using radial basis functions, Aerosp. Sci. Technol. 5 (2) (2001) 125–134, https://doi.org/10.1016/S1270-9638(00)01087-7.

[18] T.C.S. Rendall, C.B. Allen, Unified fluid-structure interpolation and mesh motion using radial basis functions, Int. J. Numer. Methods Eng. 74 (10) (2008) 1519–1559, https://doi.org/10.1002/nme.2219.

[19] G.P. Guruswamy, A review of numerical fluids/structures interface methods for computations using high-fidelity equations, Comput. Struct. 80 (1) (2002) 31–41.

[20] A. de Boer, A.H. van Zuijlen, H. Bijl, Review of coupling methods for non-matching meshes, Comput. Methods Appl. Mech. Eng. 196 (8) (2007) 1515–1525, https://doi.org/10.1016/j.cma.2006.03.017.

[21] A.L. Gaitonde, S.P. Fiddes, Three-dimensional moving mesh method for the calculation of unsteady transonic flows, Aeronaut. J. 99 (984) (1995) 150–160.

[22] G.K.W. Kenway, G.J. Kennedy, J.R.R.A. Martins, A CAD-free approach to high fidelity aerostructural optimization, in: 13^{th} AIAA/ISSMO Multidisciplinary Analysis Optimization Conference, 2010, AIAA 2010-9231.

[23] B.K. Soni, Two and three-dimensional grid generation internal flow applications, AIAA Paper 85-1526, 1985, https://doi.org/10.2514/6.1985-1526.

[24] W.T. Jones, J.A. Samareh, A grid generation system for multidisciplinary design optimization, AIAA Paper 95-1689, 1995.

[25] J.T. Batina, Unsteady Euler airfoil solutions using unstructured dynamic meshes, AIAA J. 28 (8) (1990) 1381–1388, https://doi.org/10.2514/3.25229.

[26] C. Degand, C. Farhat, A three-dimensional torsional spring analogy method for unstructured dynamic meshes, Comput. Struct. 80 (3–4) (2002) 305–316, https://doi.org/10.1016/S0045-7949(02)00002-0.

[27] M. Murayama, K. Nakahashi, K. Matsushima, Unstructured dynamic mesh for large movement and deformation, in: 40^{th} AIAA Aerospace Sciences Meeting and Exhibit, Aerospace Sciences Meetings, 2002, AIAA 2002-0122.

[28] P.I. Crumpton, M.B. Giles, Implicit time-accurate solutions on unstructured dynamic grids, Int. J. Numer. Methods Fluids 25 (11) (1997) 1285–1300.

[29] B. Palmerio, An attraction-repulsion mesh adaptation model for flow solution on unstructured grids, Comput. Fluids 23 (3) (1994) 457–506, https://doi.org/10.1016/0045-7930(94)90015-9.

[30] A. de Boer, M.S. van der Schoot, H. Bijl, Mesh deformation based on radial basis function interpolation, Comput. Struct. 85 (11–14) (2007) 784–795, https://doi.org/10.1016/j.compstruc.2007.01.013.

[31] L. Abergo, M. Morelli, A. Guardone, Aerodynamic optimization based on a discrete adjoint framework and radial basis function mesh deformation in SU2, in: AIAA Aviation Forum 2021, 2021, AIAA paper 2021-3034.

[32] B. Mi, S. Cheng, Y. Luo, H. Fan, A new many-objective aerodynamic optimization method for symmetrical elliptic airfoils by PSO and direct-manipulation-based parametric mesh deformation, Aerosp. Sci. Technol. 120 (1) (2022), https://doi.org/10.1016/j.ast.2021.107296.

[33] J.A. Samareh, Survey of shape parameterization techniques for high-fidelity multidisciplinary design optimization, AIAA J. 39 (5) (2001) 877–884, https://doi.org/10.2514/2.1391.

[34] D.J. Poole, C.B. Allen, T.C.S. Rendall, Global optimization of wing aerodynamic optimization case exhibiting multimodality, J. Aircr. 55 (4) (2018), https://doi.org/10.2514/1.C034718.

[35] B. Liu, H. Liang, Z-H. Han, G. Yang, Surrogate-based aerodynamic shape optimization of a morphing wing considering a wide Mach-number range, Aerosp. Sci. Technol. 124 (5) (2022), https://doi.org/10.1016/j.ast.2022.107557.

[36] T.M.S. Jim, G.A. Faza, P.S. Palar, K. Shimoyama, A multiobjective surrogate-assisted optimisation and exploration of low-boom supersonic transport planforms, Aerosp. Sci. Technol. 128 (9) (2022), https://doi.org/10.1016/j.ast.2022.107747.

[37] V. Raul, L. Leiffson, Surrogate-based aerodynamic shape optimization for delaying airfoil dynamic stall using Kriging regression and infill criteria, Aerosp. Sci. Technol. 111 (4) (2021), https://doi.org/10.1016/j.ast.2021.106555.

[38] J. Luo, Z. Fu, Y. Zhang, W. Fu, J. Chen, Aerodynamic optimization of a transonic fan rotor by blade sweeping using adaptive Gaussian process, Aerosp. Sci. Technol. 137 (6) (2023), https://doi.org/10.1016/j.ast.2023.108255.

[39] J.R.R.A. Martins, J. Alonso, J. Reuther, High-fidelity aerostructural design optimization of a supersonic business jet, J. Aircr. 41 (3) (2004) 523–530, https://doi.org/10.2514/1.11478.

[40] K. Leoviriyakit, Wing Planform Optimization via an Adjoint Method, PhD thesis, Stanford, 2005.

[41] G.K.W. Kenway, J.R.R.A. Martins, Multipoint high-fidelity aerostructural optimization of a transport aircraft configuration, J. Aircr. 51 (1) (2014) 144–160, https://doi.org/10.2514/1.C032150.

[42] R.P. Liem, G.K.W. Kenway, J.R.R.A. Martins, Multimission aircraft fuel-burn minimization via multipoint aerostructural optimization, AIAA J. 53 (1) (2015) 104–122, https://doi.org/10.2514/1.J052940.

[43] N. Peters, A. Wissink, J. Ekaterinaris, On the construction of a mode based reduced order model for a moving store, Aerosp. Sci. Technol. 123 (4) (2022), https://doi.org/10.1016/j.ast.2022.107484.

[44] N. Peters, A. Wissink, J. Ekaterinaris, Machine learning-based surrogate modeling approaches for fixed-wing store, Aerosp. Sci. Technol. 133 (2) (2023), https://doi.org/10.1016/j.ast.2023.108150.

[45] P.M. Zadeh, V. Toropov, Multi-fidelity multidisciplinary design optimization based on collaborative optimization framework, in: 9^{th} AIAA/ISSMO Symposium on Multidisciplinary Analysis and Optimization, Atlanta, 2002, AIAA paper 2002-5504.

[46] Y. Kishi, M. Kanazaki, Y. Makino, Supersonic forward-swept wing design using multifidelity efficient global optimization, J. Aircr. 59 (4) (2022) 1027–1040, https://doi.org/10.2514/1.C036422.

[47] O. Okumus, M. Senipek, A. Alper Ezertas, Multi-objective multi-fidelity aerodynamic optimization of helicopter rotor, in: 60^{th} AIAA Aerospace Sciences Meeting, AIAA Scitech Forum 2022, 2022, AIAA paper 2022-2099.

[48] T. Zhang, G.N. Barakos, Furqan, M. Foster, Multi-fidelity aerodynamic design and analysis of propellers for a heavy-lift eVTOL, Aerosp. Sci. Technol. 135 (4) (2023), https://doi.org/10.1016/j.ast.2023.108185.

[49] H.H. Mian, G. Wang, H. Zhou, X. Wu, Optimization of thin electric propeller using physics-based surrogate model with space mapping, Aerosp. Sci. Technol. 111 (4) (2021), https://doi.org/10.1016/j.ast.2021.106563.

[50] S. Ueda, H. Ogawa, Multi-fidelity approach for global trajectory optimization using GPU-based highly parallel architecture, Aerosp. Sci. Technol. 116 (9) (2021), https://doi.org/10.1016/j.ast.2021.106829.

[51] A. Feldstein, D. Lazzara, N. Princen, W. Willcox, Multifidelity data fusion: application to blended-wing-body multidisciplinary analysis under uncertainty, AIAA J. 58 (2) (2020), https://doi.org/10.2514/1.J058388.

[52] T.A. Reist, D.W. Zingg, M. Rakowitz, G. Potter, S. Banerjee, Multifidelity optimization of hybrid wing–body aircraft with stability and control requirements, J. Aircr. 56 (2) (2019), https://doi.org/10.2514/1.C03470.

[53] S.G. Kontogiannis, M.A. Savill, T. Kipouros, Multiobjective aerostructural optimization for efficient transport wing conceptual design, in: 59^{th} AIAA/ASCE/AHS/ASC Structures, Structural Dynamics, and Materials Conference, AIAA SciTech Forum, Kissimmee, Florida, 2018, AIAA Paper 2018-0104.

[54] S.G. Kontogiannis, M.A. Savill, A Generalized Methodology for Multidisciplinary Design Optimization Using Surrogate Modelling and Multifidelity Analysis, Optimization in Engineering, Springer, 2019, OPTE-2019-752.

[55] J. Vassberg, M. Dehaan, M. Rivers, R. Wahls, Development of a common research model for applied CFD validation studies, in: 26^{th} AIAA Applied Aerodynamics Conference, Guidance, Navigation, and Control and Co-Located Conferences, 2008, AIAA 2008-6919.

[56] A.I.J. Forrester, A.J. Keane, Recent advances in surrogate based optimization, Prog. Aerosp. Sci. 45 (1–3) (2009) 50–79, https://doi.org/10.1016/j.paerosci.2008.11.001.

[57] S.G. Kontogiannis, M.A. Savill, T. Kipouros, A multi-objective multi-fidelity framework for global optimization, in: 58^{th} AIAA/ASCE/AHS/ASC Structures, Structural Dynamics, and Materials Conference, AIAA SciTech Forum, 2017, AIAA Paper 2017-0136.

[58] R.E. Perez, P.W. Janses, J.R.R.A. Martins, pyOpt: a Python-based object-oriented framework for nonlinear constrained optimization, Struct. Multidiscip. Optim. 45 (1) (2012) 101–118, https://doi.org/10.1007/s00158-011-0666-3.

[59] D.R. Jones, A taxonomy of global optimization methods based on response surfaces, J. Glob. Optim. 21 (4) (2001) 345–383, https://doi.org/10.1023/A:1012771025575.

[60] A.I.J. Forrester, A. Sobester, A.J. Keane, Engineering Design via Surrogate Modelling: A Practical Guide, John Wiley & Sons, ISBN 978-0-470-06068-1, 2008.

[61] J.E. Alvarez-Benitez, R.M. Everson, J.E. Fieldsend, A MOPSO algorithm based exclusively on Pareto dominance concepts, in: International Conference on Evolutionary Multi-Criterion Optimization EMO 2005: Evolutionary Multi-Criterion Optimization, vol. 3410, 2005, pp. 459–473.

[62] S.G. Kontogiannis, J. Demange, M.A. Savill, T. Kipouros, A comparison study of two multifidelity methods for aerodynamic optimization, Aerosp. Sci. Technol. 97 (2) (2020), https://doi.org/10.1016/j.ast.2019.105592.

[63] O. Dababneh, A. Kayran, Design, analysis and optimization of thin walled semi-monocoque wing structures using different structural idealization in the preliminary design phase, Int. J. Struct. Integr. 5 (3) (2014) 214–226, https://doi.org/10.1108/IJSI-12-2013-0050.

[64] T.W. Sederberg, S.R. Parry, Free-form deformation of solid geometric models, ACM 20 (2) (1986) 151–160, https://doi.org/10.1145/15922.15903.

[65] ANSYS FLuent 14.5, User's Manual, ANSYS Inc.

[66] A.I.J. Forrester, N.W. Bressloff, A.J. Keane, Optimization using surrogate models and partially converged computational fluid dynamics simulations, Proc. R. Soc. A, Math. Phys. Eng. Sci. 462 (2071) (2006) 2177–2204, https://doi.org/10.1098/rspa.2006.1679.

[67] P.L. Roe, Approximate Riemann solvers, parameter vectors and difference schemes, J. Comput. Phys. 43 (2) (1981) 357–372, https://doi.org/10.1016/0021-9991(81)90128-5.

[68] D.C. Wilcox, Turbulence Modeling for CFD, 3rd ed., DCW Industries, La Cãnada, Calif., 2006, ISBN-10: 1928729088.

[69] S. Kontogiannis, Conceptual Multidisciplinary Design via a Multiobjective Multifidelity Optimisation Method, PhD thesis, Cranfield University, 2018.

[70] O. Dababneh, Multidisciplinary Design Optimisation for Aircraft Wing Mass Estimation, PhD Thesis, Cranfield University, April 2016.

[71] T.F. Wunderlich, S. Dähne, L. Reimer, A. Schuster, Global aerostructural design optimization of more flexible wings for commercial aircraft, J. Aircr. 58 (6) (2021), https://doi.org/10.2514/1.C03470.

[72] A.C. Gray, J.R.R.A. Martins, Geometrically nonlinear high-fidelity aerostructural optimization for highly flexible wings, in: 59^{th} AIAA Aerospace Sciences Meeting, AIAA Scitech Forum 2021, 2021, AIAA paper 2021-0283.

[73] J.D. Taylor, Jeffrey D. Taylor, D.F. Hunsakerh, Characterization of the common research model wing for low-fidelity aerostructural analysis, in: 59^{th} AIAA Aerospace Sciences Meeting, AIAA Scitech Forum 2021, 2021, AIAA paper 2021-1591.
[74] ANSA v17.1.0 Theory Guide, Beta CAE Systems, 2016.
[75] J. Demange, M. Savill, T. Kipouros, Multifidelity optimization for high-lift airfoils, in: 54^{th} AIAA Aerospace Sciences Meeting, AIAA Scitech Forum 2016, San Diego, 2016, AIAA paper 2016-0557.
[76] M.C. Niu, Airframe Structural Design, Conmilit Press Limited, Hong Kong, ISBN 962712804X, 1988.
[77] J.R.R.A. Martins, A.B. Lambe, Multidisciplinary design optimization: a survey of architectures, AIAA J. 51 (9) (2013) 2049–2075, https://doi.org/10.2514/1.J051895.



https://dspace.org/

Multiobjective aerostructural optimization for efficient transport wing conceptual design

Kontogiannis, Spyridon G.; Savill, Mark A.; Mazis, Vasileios; Skaperdas, Vangelis

2024-05-01
Elsevier
https://doi.org/10.1016/j.ast.2024.109080
Kontogiannis SG, Savill AM, Mazis V, Skaperdas V. (2024) Multiobjective aerostructural optimization for efficient transport wing conceptual design. Aerospace Science and Technology, Volume 148, May 2024, Article number 109080

Downloaded from a DSpace repository. https://dspace.org/